

[SiO_2 nanoparticle-regulated crystallization of lead halide perovskite and improved efficiency of carbon-electrode-based low-temperature planar perovskite solar cells]

Zerong Liang(梁泽荣), Bingchu Yang(杨兵初), Anyi Mei(梅安意), Siyuan Lin(林思远), Hongwei Han(韩宏伟), Yongbo Yuan(袁永波), Haipeng Xie(谢海鹏), Yongli Gao(高永立), Conghua Zhou(周聪华)

Citation: Chin. Phys. B . 2020, 29(7): 078401 . **doi:** 10.1088/1674-1056/ab8da5
Journal homepage: http://cpb.iphy.ac.cn; http://iopscience.iop.org/cpb

What follows is a list of articles you may be interested in

[Factors influencing the performance of paintable carbon-based perovskite solar cells fabricated in ambient air]

Wei-Kang Xu(许伟康), Feng-Xiang Chen(陈凤翔), Gong-Hui Cao(曹功辉), Jia-Qi Wang(王嘉绮), Li-Sheng Wang(汪礼胜)
Chin. Phys. B . 2018, 27(3): 038402 . **doi:** 10.1088/1674-1056/27/3/038402

[Importance of ligands on TiO_2 nanocrystals for perovskite solar cells]

Yao Zhao(赵耀), Yi-Cheng Zhao(赵怡程), Wen-Ke Zhou(周文可), Rui Fu(伏睿), Qi Li(李琪), Da-Peng Yu(俞大鹏), Qing Zhao(赵清)
Chin. Phys. B . 2018, 27(1): 018401 . **doi:** 10.1088/1674-1056/27/1/018401

[Improving power conversion efficiency of perovskite solar cells by cooperative LSPR of gold-silver dual nanoparticles]

Peng Liu(刘鹏), Bing-chu Yang(杨兵初), Gang Liu(刘钢), Run-sheng Wu(吴闰生), Chu-jun Zhang(张楚俊), Fang Wan(万方), Shui-gen Li(李水根), Jun-liang Yang(阳军亮), Yong-li Gao(高永立), Cong-hua Zhou(周聪华)
Chin. Phys. B . 2017, 26(5): 058401 . **doi:** 10.1088/1674-1056/26/5/058401

[Alleviating hysteresis and improving device stability of perovskite solar cells via alternate voltage sweeps]

Chao Xia(夏超), Wei-Dong Song(宋伟东), Chong-Zhen Zhang(张崇臻), Song-Yang Yuan(袁松洋), Wen-Xiao Hu(胡文晓), Ping Qin(秦萍), Ru-Peng Wang(王汝鹏), Liang-Liang Zhao(赵亮亮), Xing-Fu Wang(王幸福), Miao He(何苗), Shu-Ti Li(李述体)
Chin. Phys. B . 2017, 26(1): 018401 . **doi:** 10.1088/1674-1056/26/1/018401

[Improving the performance of perovskite solar cells with glycerol-doped PEDOT:PSS buffer layer]

Jian-Feng Li(李建丰), Chuang Zhao(赵创), Heng Zhang(张恒), Jun-Feng Tong(同军锋), Peng Zhang(张鹏), Chun-Yan Yang(杨春燕), Yang-Jun Xia(夏养君), Duo-Wang Fan(范多旺)
Chin. Phys. B . 2016, 25(2): 028402 . **doi:** 10.1088/1674-1056/25/2/028402

SiO_2 nanoparticle-regulated crystallization of lead halide perovskite and improved efficiency of carbon-electrode-based low-temperature planar perovskite solar cells*

Zerong Liang(梁泽荣)[1], Bingchu Yang(杨兵初)[1,†], Anyi Mei(梅安意)[2], Siyuan Lin(林思远)[1], Hongwei Han(韩宏伟)[2], Yongbo Yuan(袁永波)[1], Haipeng Xie(谢海鹏)[1], Yongli Gao(高永立)[1,3], and Conghua Zhou(周聪华)[1,‡]

[1] *Hunan Key Laboratory of Super-microstructure and Ultrafast Process, School of Physics and Electronics, Central South University, Changsha* 410083, *China*
[2] *Michael Grätzel Center for Mesoscopic Solar Cells, Wuhan National Laboratory for Optoelectronics, Huazhong University of Science and Technology, Wuhan* 430074, *China*
[3] *Department of Physics and Astronomy, University of Rochester, Rochester, NY* 14627, *USA*

(Received 5 March 2020; revised manuscript received 20 April 2020; accepted manuscript online 28 April 2020)

SiO_2 nanoparticles were used to regulate the crystallizing process of lead halide perovskite films prepared by the sequential deposition method, which was used in the low-temperature-processed, carbon-electrode-basing, hole-conductor-free planar perovskite solar cells. It was observed that, after adding small amount of SiO_2 precursor (1 vol%) into the lead iodide solution, performance parameters of open-circuit voltage, short-circuit current and fill factor were all upgraded, which helped to increase the power conversion efficiency (reverse scan) from 11.44(±1.83)% (optimized at 12.42%) to 14.01(±2.14)% (optimized at 15.28%, AM 1.5G, 100 mW/cm^2). Transient photocurrent decay curve measurements showed that, after the incorporation of SiO_2 nanoparticles, charge extraction was accelerated, while transient photovoltage decay and dark current curve tests both showed that recombination was retarded. The improvement is due to the improved crystallinity of the perovskite film. X-ray diffraction and scanning electron microscopy studies observed that, with incorporation of amorphous SiO_2 nanoparticles, smaller crystallites were obtained in lead iodide films, while larger crystallites were achieved in the final perovskite film. This study implies that amorphous SiO_2 nanoparticles could regulate the coarsening process of the perovskite film, which provides an effective method in obtaining high quality perovskite film.

Keywords: perovskite solar cell, carbon-electrode, crystallization, low temperature, SiO_2, lead iodide

PACS: 84.60.Jt, 88.40.H–, 88.40.HJ, 81.10.–h **DOI:** 10.1088/1674-1056/ab8da5

1. Introduction

Perovskite solar cells (PSCs) have attracted a great deal of attention due to their rapid development of photo-to-electric power conversion efficiency (PCE). The efficiency has increased from 3.8% in 2009[1] to the latest 25.2%,[2] which is appealing for the potential commercialization. However, it has been seriously hampered by two problems, price and stability. Usually these PSCs use precious metals (such as Au, Ag, and Cu[3–5]), and expensive hole-transporting materials (HTMs, such as PTAA[3] and spiro-OMeTAD[6]). This not only increases the manufacturing costs, but also affects device stability. Replacing metal electrodes and HTMs by carbon-electrode could help to solve these problems, since the latter is cheap in price, inert to electrochemical corrosion, highly conductive and holding suitable work function (∼5.0 eV). These merits trigger the so-called carbon-electrode-based PSCs (CPSCs, and often "hole-conductor-free" is titled). Since the pioneered mesoscopic CPSCs proposed by Han's group,[7,8] until now several structures have been proposed, for example, embedment,[9,10] quasi-planar,[11,12] and planar CPSCs.[13] These devices have shown excellent stability. However, the power conversion efficiencies (PCEs) of these CPSCs are right now relatively lower than those of devices based on metal-electrodes, thus it is essential to be upgraded.[14] To improve the device performance, healing the interface between perovskite and carbon electrode was observed to be helpful due to the accelerated charge transfer.[13,15,16] On the other hand, bulk engineering also works. In the studies of metal-electrode-based PSCs, improving crystallinity of the active layer or the lead halide perovskite (PVSK for short) is found to be the key to obtain higher efficiencies. Several strategies have been proposed. For example, in 2014, Huang and co-workers found that, solvent annealing could improve the crystallinity of $MAPbI_3$ ($MA = CH_3NH_3$) and thus the device performance.[17] You *et al.* observed that moisture-assisted annealing was also useful to the crystallization of the MA-based perovskite.[18] For FA [$CH(NH_2)_2$]-based perovskite, several studies showed that importing small ions such as MA^+,

*Project supported by the Fundamental Research Funds for the Central South University, China (Grant No. 2019zzts426), the National Natural Science Foundation of China (Grant Nos. 61172047, 61774170, and 51673218), the Scientific and Technological Project of Hunan Provincial Development and Reform Commission, China, the National Science Foundation, USA (Grant Nos. CBET-1437656 and DMR-1903962), and the Innovation-Driven Project of Central South University (Grant No. 2020CX006).

†Corresponding author. E-mail: bingchuyang@csu.edu.cn
‡Corresponding author. E-mail: chzhou@csu.edu.cn

© 2020 Chinese Physical Society and IOP Publishing Ltd

Rb^+, Cs^+, K^+, Cl^-, Br^- could facilitate the nucleation and growth of the desirable α-$FAPbI_3$ (black phase).[19–23] Impressively, Han *et al.* in 2014 reported that solvent additive of dimethyl sulfoxide (DMSO) could retard the crystallinity of the PbI_2, which then led to improved crystallization of $MAPbI_3$ in sequential formation routine.[24] Chen *et al.* observed that intermediate phase could be formed between DMSO and PbI_2, which favored the formation of PVSK crystallites.[25,26] On the other hand, porous structured PbI_2 films could improve the crystallinity of PVSK films,[27–29] while adding polymers or nanomaterials into the perovskite precursor could also favor the crystallizing process of photoactive materials.[30–35]

As an alternative, in this work, SiO_2 nanoparticles (SiO_2 NPs thereafter) were mixed with PbI_2 solution, aiming at favoring the crystallization process of PVSK ($FA_{0.75}MA_{0.25}PbI_{2.81}Cl_{0.19}$) and thus improve performance of carbon-electrode-based devices. As will be shown later, these nanoparticles could retard the crystallinity of PbI_2 films, through which crystallinity of resultant PVSK films can be upgraded. The improved crystallinity then upgrades the device efficiency of the low-temperature planar CPSCs from <15%[13] to 15.28% (reverse scan, AM1.5G, 100 mW/cm^2, corresponding to 14.46% for the maximum power point tracking).

2. Experimental section

2.1. Materials

Carbon black (99%, Sinopharm), graphite (99.8%, Sinopharm), zirconium oxide (ZrO_2, 99%, Sinopharm), SiO_2 nanoparticles (A380, Degussa), hydroxypropyl cellulose (HPC, M.W. = 100000, Aladdin), tin (II) chloride dehydrate ($SnCl_2{\cdot}H_2O$, 98%, Sinopharm), lead iodide (PbI_2, 99.99%, Xi'an Polymer Light Technology Corp.), formamidinium iodide [$HC(NH_2)_2I$, FAI, 99.5%, Xi'an Polymer Light Technology Corp.], methylammonium bromide (CH_3NH_3Br, MABr, Xi'an Polymer Light Technology Corp.), methylammonium chloride (CH_3NH_3Cl, MACl, 99.5%, Xi'an Polymer Light Technology Corp.), anhydrous N,N-dimethylformamide (DMF, 99.9%, Sigma), isopropyl alcohol (IPA, 99%, Sigma), acetone (99%, Sinopharm), dimethyl sulfoxide (DMSO, 99.8%, Sigma), ethanol (99%, Sinopharm), terpineol (95%, Sinopharm) were purchased from market, and the received samples were used without further purification. Deionized water was prepared in laboratory.

2.2. Fabrication of the carbon-electrode-based low-temperature planar perovskite solar cells

In our experiment, 2 g SiO_2 nanoparticles were dispersed in 10 mL DMF and filtered so as to remove the large particles. The obtained SiO_2 precursor solution was then added into PbI_2 solvent as DMF, for example, 1% SiO_2 precursor was 10 μL SiO_2 precursor + 890 μL DMF + 100 mL DMSO. Carbon paste was prepared as follows: carbon black powder (2 g), graphite powder (6 g), ZrO_2 powder (1 g), hydroxypropyl cellulose (1 g) and terpineol (30 mL) were mixed by ball milling at 300 rpm for 24 h. FTO substrates were ultrasonically cleaned in deionized water, acetone, isopropyl alcohol each for 10 min, dried in oven, and then further treated in UV-ozone for 20 min. An SnO_2 layer was prepared as follows: $SnCl_2{\cdot}H_2O$ solution (0.1 mol/L in ethanol) was spin-coated on FTO using speed of 3000 rpm (30 s), followed by heat-treating on hot plate at 150 °C for 1 h and UV-ozone irradiation for 20 min. A perovskite layer was prepared using the so-called sequential method. Firstly, PbI_2 solution (1.5 mol/L in mixed solvents of DMF and DMSO, with volume ratio of 9 : 1 (DMF:DMSO) was spin-coated on the as-coated SnO_2 film at 3000 rpm for 30 s, and then annealed at 70 °C for 1 min. Secondly, mixture solution of $FAI_{0.75}MAI_{0.06}MACl_{0.19}$ (M_{FAI}:M_{MAI}:M_{MACl} = 90 mg : 6.38 mg : 9 mg, dissolved in 1 ml isopropanol) was spin-coated on top of the PbI_2 film (2000 rpm for 20 s), and annealed at 140 °C for 20 min to obtain the PVSK film. Finally, a carbon electrode was deposited by doctor-blading the carbon paste on top of the perovskite film, and dried at 100 °C for 30 min, after which the devices are ready for performance evaluation.

2.3. Material characterization and device performance evaluation

Morphological properties of the lead iodide and perovskite films were characterized by high-resolution transmission electron microscopy (HR-TEM, model G2 f20) and scanning electron microscopy (SEM, TESCAN MIRA3 LUM), respectively. In addition, element distribution of the films was studied by energy dispersive x-ray spectroscopy (EDX) affiliated to the SEM. Crystallographic properties of materials were characterized x-ray diffraction (XRD, D500, Siemens). X-ray photoemission spectroscopy (XPS, SPECS XR-MF) of the materials was characterized using a monochromatized Al source with $h\nu$ of 1486.6 eV and incidence angle of 54° (resolution of the spectrometer is 70 meV). Current-voltage curves of the low-temperature CPSCs were recorded by a digital sourcemeter (model 2400, Keithley Inc.) under simulated illumination (AM1.5G, 91160S, Newport) with intensity of 100 mW/cm^2 (before test, the intensity was calibrated by standard silicon cell SRC-1000-TC-QZ-N, Oriel). Transient photovoltage/photocurrent (TPV/TPC) decay curves were measured by a home-made system including a digital oscilloscope (Keysight DSO-X 3104A) and N_2 laser (NL100, 337 nm, Stanford). For TPV measurement, background illumination was used to generate open circuit voltage (V_{OC}) of about 950 mV, then laser pulse was imported to generate small ΔV_{OC} which was less than 5% of the background V_{OC}. Ex-

ternal quantum efficiency (EQE) was tested by spectrum performance testing system (7-SCSpec, Beijing) with AC mode (14 Hz). Storage stability of the devices was tested by storing the devices in dark [ambient, with relative humidity of 45(±10)%, no encapsulation was used]. Periodic test was performed to evaluate the storage stability.

3. Results and discussion

Fabrication process of the low-temperature planar CPSCs is shown in Fig. 1(a), following the protocol described in the previous work.[13] A sandwiched structure of "FTO/SnO_2/PVSK/C" is adopted (as shown by the typical cross-sectional SEM image in Fig. S1). To make it compatible with the low temperature procedures, treating temperature of the SnO_2 layer was reduced from the previously adopted 180 °C to the currently used 150 °C.[13] To tune the crystallization of both PbI_2 and afterwards PVSK films, trace amount of SiO_2 NPs was imported to the system by mixing SiO_2 precursor (1 g/10 mL) into PbI_2 solution with varied volume ratios, or 0, 0.1%, 1%, 10%, etc. To help discussion, the volume ratio between SiO_2 NPs and PbI_2 is also estimated, for example, it is about 1/2570 when volume ratio of SiO_2 precursor is 0.1%. As a result, expansion effect of the SiO_2 NPs could be neglected. For comparison, x-ray diffraction study was performed on these SiO_2 NPs. As is expected, these nanoparticles are mainly amorphous when considering the low intensity. Transmission electron microscope (TEM) image in Fig. 1(c) shows that the SiO_2 NPs are well-dispersed, with particle sizes of about 10 nm.

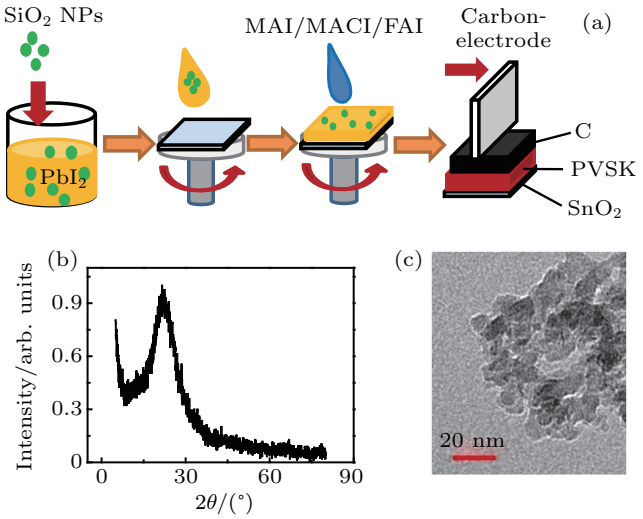


Fig. 1. (a) Schematic figures for the preparation of low temperature, planar CPSCs with addition of SiO_2 NPs in PbI_2 solution. (b) XRD pattern of the SiO_2 NPs. (c) TEM image of the SiO_2 NPs.

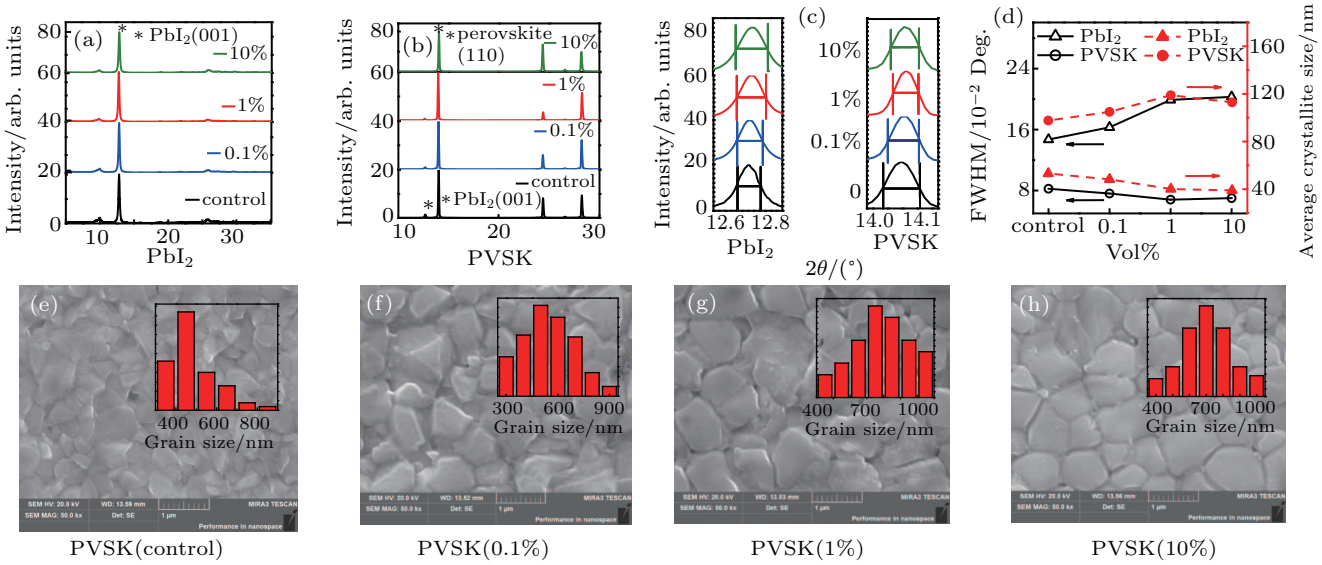


Fig. 2. XRD patterns of (a) PbI_2 and (b) PVSK films with addition of SiO_2 NPs (volume ratios of the SiO_2 precursor were marked). (c) Enlarged diffraction peaks of PbI_2 (001) and PVSK (110) [dashed lines show the full width at half maximum (FWHM) of each peak]. (d) Effect of SiO_2 NPs on the average crystallite size of PbI_2 and PVSK. (e)–(h) Typical scanning electron microscopy images of PVSK films with addition of SiO_2 NPs. Distribution histograms of grain sizes are shown in inset of the images.

Effect of SiO_2 NPs on the crystallization behavior of PbI_2 and the afterwards-formed PVSK films were studied. XRD study showed that adding SiO_2 NPs could retard the crystallization of PbI_2. As seen in Fig. 2(c), with volume ratio of the SiO_2 precursor, the FWHM of the peak of PbI_2 (001) increases; while for the PVSK films, the FWHM decreases. To show it more clearly, average crystallite size is calculated by Scherrer's formula using the FWHM peaked. As shown in Fig. 2(d), opposite trends are illustrated. With amount of SiO_2 NPs increases, PbI_2 crystallites tend to be smaller, while PVSK crystallites become larger. The improved crystallization of PVSK could also be reflected from morphology studies. As shown by the scanning electron microscopy (SEM) images, with increase of the volume ratio of SiO_2 NPs, larger PVSK grains could be harvested. For example, average grain size is around 500 nm before SiO_2 incorporation, but increases

to be around 700 nm after adding 1% (volume ratio) SiO_2 precursor into PbI_2 solution. The SiO_2 NPs distributed uniformly in both of the PbI_2 and PVSK films, as being reflected by EDS mapping (Figs. S2 and S3). The above studies tell us that SiO_2 NPs have retarded the crystallization of PbI_2, but favored the crystallization of PVSK.

The improved crystallinity of the PVSK could also be reflected by absorption behavior and the lifetime measurement. UV-vis absorption spectra in Fig. 3(a) show that, after incorporation of SiO_2 NPs, extinction of PVSK is improved, while time-resolved photoluminescence (TRPL) in Fig. 3(b) shows that lifetime of the photo-generated charge-carriers is increased after incorporation of SiO_2 NPs. The prolonged lifetime would be helpful for the power conversion of the perovskite solar cells.

From the above studies one could see that retarding the crystallization of PbI_2 is beneficial to obtain higher quality PVSK films. The regulated crystallite growth of PVSK could be well understood by considering the interaction between SiO_2 and PbI_2. X-ray photoemission spectroscopy test in Fig. 4(a) reflects that, after incorporation of SiO_2 NPs, binding energies of both Pb 4f and I 3d shifted, indicating possible interaction between them. For better illustration about the regulation brought by SiO_2 NPs, schematics are drawn in Fig. 4(b). Due to the disruption brought by SiO_2 NPs, crystallization process of PbI_2 is affected. Thus the PbI_2 film tends to be more amorphous, which is beneficial to the crystallization process of the afterwards-growing PVSK film. Since the amorphous state of PbI_2 makes it easier for organic ions (like FA^+, MA^+, I^-, etc.) to diffuse and react with PbI_2.[27,29,36] It is worth noting that the SiO_2 NPs had not obviously modified the film morphology of PbI_2. This is different from the result revealed by Yi *et al.*, who observed that porous structure could be brought by evaporating DMSO in fresh PbI_2 films.[28] Here it is shown that the amorphous SiO_2 NPs could retard the crystallization of PbI_2, which is similar to that brought by DMSO as proposed by Han *et al.*[24] Thus one more strategy is provided to regulate the crystallization process of the PVSK films.

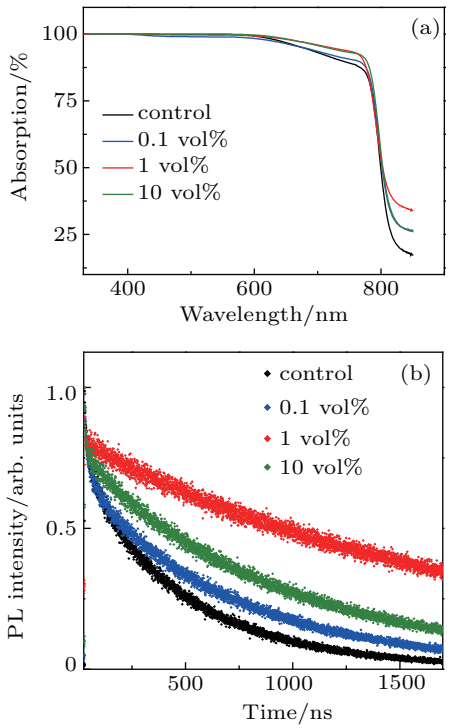


Fig. 3. (a) UV-vis absorption spectra, and (b) time-resolved photoluminance spectra (TRPL) of PVSK films with incorporation of SiO_2 NPs.

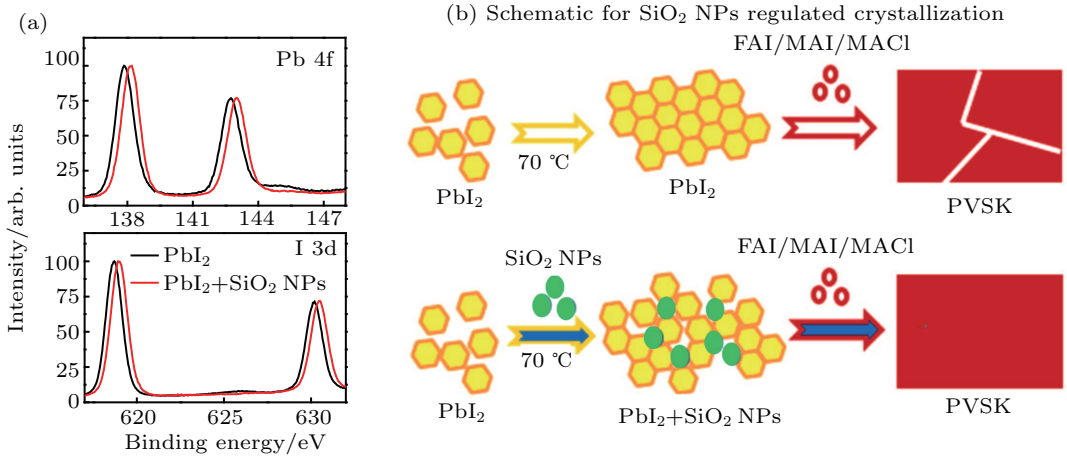


Fig. 4. (a) X-ray photoemission spectra of PbI_2 films with or without incorporation of SiO_2 NPs. (b) Schematic of the effect of SiO_2 NPs on regulated crystallization of PVSK film.

It was observed that adding small amount of SiO_2 NPs into PbI_2 solution (and then the PVSK films) could upgrade device efficiency of the low-temperature planar CPSCs. As reflected by the typical current density–voltage (J–V) curves shown in Fig. 5(a), the corresponding performance parameters including open-circuit voltage (V_{OC}), short-circuit current density (J_{SC}), fill factor (FF) and power conversion efficiency (PCE) are also listed in Table 1. It was observed that addition of SiO_2 NPs upgrades J_{SC}, V_{OC} and FF in all. For better illustration, these three performance parameters, as well as the PCE, are all collected and plotted against the volume ratio of SiO_2 precursor in Fig. 5(b). About 20 separated de-

vices were used. Compared with the control devices (w/o SiO_2 NPs), all of the four parameters have been upgraded, especially for the case of moderate ratio of 1%. Concretely, FF increases from 52.92(±9.64)% to 61.17(±8.37)%, J_{SC} increases from 23.05(±0.55) mA/cm^2 to 23.51(±0.63) mA/cm^2, V_{OC} increases from 0.949(±0.019) V to 0.988(±0.014) V, these help to upgrade PCE from 11.44(±1.83)% to 14.01(±2.14)%, with the optimized at 15.28% (Fig. S4).

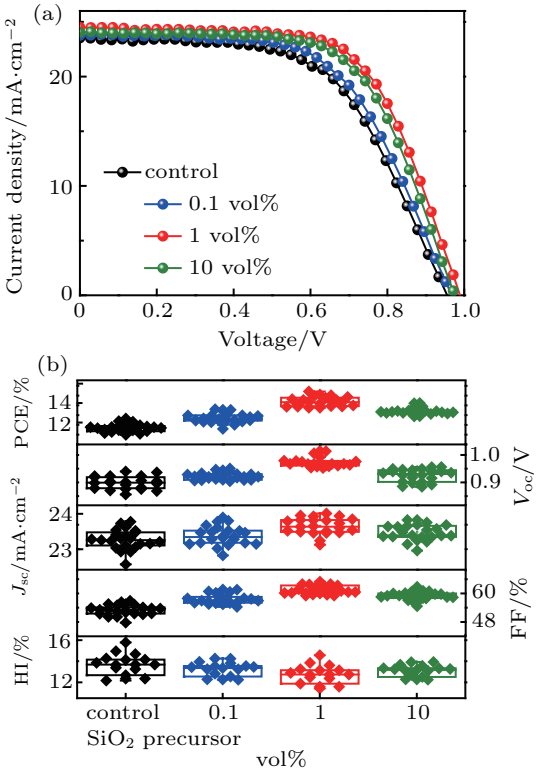


Fig. 5. (a) Typical current density–voltage (J–V) curves of as-fabricated devices recorded from reverse scan under simulated illumination (AM 1.5G, 100 mW/cm^2, testing area is 0.0514 cm^2). (b) Effect of volume ratio of SiO_2 precursor on the performance parameters (reverse scan) and hysteresis index (HI).

To verify the improvement in photocurrent, external quantum efficiency (EQE) tests were performed. As shown in Fig. S5, the similar trend is observed in the integrated current density. Hysteresis behavior is also examined by collecting the PCEs from both reverse/forward scans. Hysteresis index (HI) factors are calculated using the method described before.[6] As shown in bottom of Fig. 5(b), incorporation of SiO_2 NPs is also favorable to reach lower hysteresis. HI decreases slightly from 13.69(±3.29)% to 12.72(±2.24)% (ratio of 1%).

Table 1. Performance parameters picked from the J–V curves in Fig. 5(a).

SiO_2 precursor/vol%	V_{OC}/V	J_{SC}/mA·cm^{-2}	FF/%	PCE/%
0	0.954	22.91	54.77	11.97
0.1	0.968	23.18	57.18	12.83
1	0.987	23.83	61.94	14.57
10	0.977	23.22	61.53	13.96

Charge transport and recombination dynamics of the low-temperature planar CPSCs were explored with respect to the addition of SiO_2 NPs, based on transient photocurrent/voltage (TPC/TPV) decay curves tested. Typical TPC/TPV curves are shown in Fig. S6. For comparison, extraction time (t_d) and lifetime (τ) of photo-generated carriers were picked from these transient decay curves, which are shown in Figs. 6(a) and 6(b), respectively. Similar to those performed in device performance parameters, statistics were also performed. It could be clearly seen that importing SiO_2 NPs could accelerate charge transport, while retard recombination processes of the photo-generated charge carriers. Take charge extraction time t_d as an example, it starts from 12.84(±1.71) μs of the control devices (without addition of SiO_2 NPs), and decreases to 11.55(±1.10) μs, 6.75(±1.49) μs after adding SiO_2 NPs at volume ratios of 0.1% and 1%. As for life time (τ), it begins at 10.68(±3.00) μs of the control devices, and prolongs to 15.13(±4.55) μs, 56.24(±11.9) μs for volume ratios of 0.1% and 1%, respectively. The case of 1% comes out with smallest extraction time (t_d) and longest life time (τ). Comparing Figs. 6(a) and 6(b) to the performance parameters in Fig. 6(c) could find that the evolution trend of t_d is opposite to J_{SC}, while the trend of lifetime τ is in parallel with V_{OC}. Such a phenomenon is quite similar to the previous studies.[21] Thus accelerating charge extraction is beneficial to the output of photocurrent, while prolonged lifetime is favorable to output of V_{OC}.[37] The prolonged lifetime is due to the reduced recombination. This could also be reflected by dark current test. As shown in Fig. 6(c), at given bias, devices with incorporation of SiO_2 NPs produce lower dark current. Additionally the case of volume ratio 1% comes out with lowest dark current.

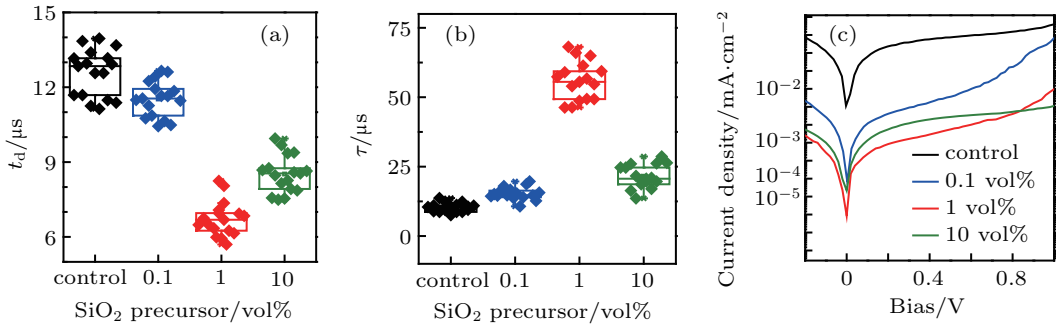


Fig. 6. Effect of volume ratio of SiO_2 precursor on (a) charge extraction time [t_d, extracted from transient photocurrent (TPC) decay curves], (b) lifetime [τ, extracted from transient photocurrent (TPV) decay curves], and (c) dark current density–voltage curves of the low-temperature planar CPSCs.

Storage stability and maximum-power-point tracking (MPPT) were tested at ambient air and in dark, with RH of about 45%, and no encapsulation was used.[13] As shown in Fig. 7(a), besides the slight increase in the first 30 days, the device efficiency changed slowly in the afterwards 100 days, showing sound storage stability of the low-temperature planar CPSCs. As for the increase in the starting 30 days, it may be ascribed to the slow-strengthening contact between the PVSK film and the top carbon electrode.[13] Careful examination in Fig. 7(b) could observe that devices assembled with SiO_2 NPs-regulated PVSK films come out with better stability. Photo-stability was also measured. Similar to the storage stability, the device assembled from the SiO_2 NP-regulated PVSK film comes out with better stability. The improved stability is ascribed to the upgraded crystallization of the PVSK films. As stated above, with incorporation of moderate amount of SiO_2 NPs, larger crystallites and also larger grains were obtained, which reduced the defects in the PVSK films, and thus favored the stability of the device system. As a result, higher crystallinity of the PVSK film is favorable to device stability.

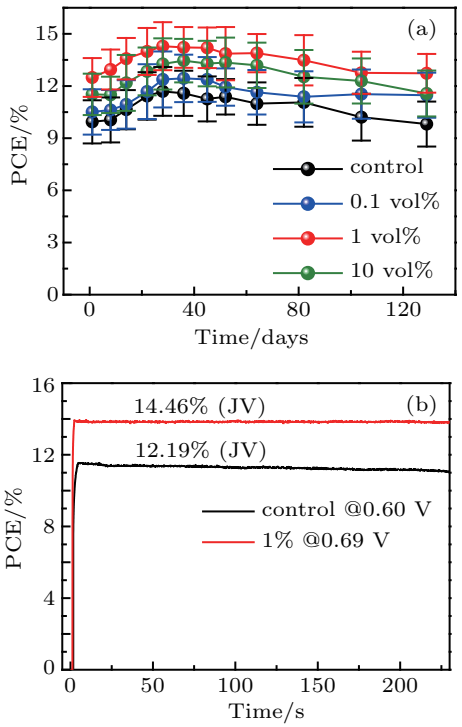


Fig. 7. Stability test of the low-temperature, carbon-electrode-based PSCs. (a) Storage stability and (b) photo-stability or the test of so-called maximum-power-point tracking (MPPT). No encapsulation was used, and for storage-test, the devices were stored at dark with relative humidity of 45%(±10%).

4. Conclusion

Finally, it comes to show that SiO_2 NPs could retard the crystallization process of PbI_2 films, making them more amorphous and also easier for the organic ions to diffuse in reaction with PbI_2. Such a strategy is verified to be effective in achieving better crystallinity of PVSK, and helpful in accelerating charge transport and retarding recombination process, and then upgrading the device performance of the low-temperature-processed carbon-electrode-based planar perovskite solar cells. This work provides an effective method in regulating the crystallization of the PVSK.

References

[1] Kojima A, Teshima K, Shirai Y and Miyasaka T 2009 *J. Am. Chem. Soc.* **131** 6050

[2] National Renewable Energy Laboratory, https://www.nrel.gov/pv/assets/pdfs/pv-efficiency-chart. 20200311.pdf

[3] Ryu S, Noh J H, Jeon N J, Kim Y C, Yang W S, Seo J and Seok S I 2014 *Energy Environ. Sci.* **7** 2614

[4] Zhao J J, Zheng X, Deng Y H, Li T, Shao Y C, Gruverman A, Shield J and Huang J S 2016 *Energy Environ. Sci.* **9** 3650

[5] Wu W Q, Wang Q, Fang Y J, Shao Y C, Tang S, Deng Y H, Lu H D, Liu Y, Li T, Yang Z B, Gruverman A and Huang J S 2018 *Nat. Commun.* **9** 1625

[6] Liu G, Zhou C H, Wan F, Li K M, Yuan Y B, Gao Y L, Lu Y, Yang B C 2018 *Appl. Phys. Lett.* **113** 113501

[7] Xu M, Rong Y G, Ku Z L, Mei A Y, Liu T F, Zhang L J, Li X and Han H W 2014 *J. Mater. Chem. A* **2** 8607

[8] Mei A Y, Li X, Liu L F, Ku Z L, Liu T F, Rong Y G, Xu M, Hu M, Chen J Z, Yang Y, Grätzel M and Han H W 2014 *Science* **345** 295

[9] Wei Z, Yan K Y, Chen H N, Yi Y, Zhang T, Long X, Li J K, Zhang L X, Wang J N and Yang S H 2014 *Energy Environ. Sci.* **7** 3326

[10] Yang Y L, Liu Z H, Ng W K, Zhang L H, Zhang H, Meng X Y, Bai Y, Xiao S, Zhang T, Hu C, Wong K S and Yang S H 2019 *Adv. Funct. Mater.* **29** 1806506

[11] Meng X Y, Zhou J S, Hou J, Tao X, Cheung S H, So S K and Yang S H 2018 *Adv. Mater.* **30** 1706975

[12] Wei H Y, Xiao J Y, Yang Y Y, Lv S T, Shi J J, Xu X, Dong J, Luo Y H, Li D M and Meng Q B 2015 *Carbon* **93** 861

[13] Yan J Q, Lin S Y, Qiu X C, Chen H, Li K M, Yuan Y B, Long M Q, Yang B C, Gao Y L and Zhou C H 2019 *Appl. Phys. Lett.* **114** 103503

[14] Zhou C H and Lin S Y 2019 *Solar RRL* **4** 1900190

[15] Liu T F, Liu L F, Hu M, Yang Y, Zhang L J, Mei A Y and Han H W 2015 *J. Power Sources* **293** 533

[16] Xu W K, Chen F X, Cao G H, Wang J Q and Wang L S 2018 *Chin. Phys. B* **27** 038402

[17] Xiao Z G, Dong Q F, Bi C, Shao Y C, Yuan Y B and Huang J S 2014 *Adv. Mater* **26** 6503

[18] You J B, Yang Y, Hong Z R, Song T B, Meng L, Liu Y S, Jiang C Y, Zhou H P, Chang W H and Li G 2014 *Appl. Phys. Lett.* **105** 183902

[19] Saliba M, Matsui T, Seo J Y, Domanski K, Correa-Baena J P, Nazeeruddin M K, Zakeeruddin S M, Tress W, Abate A, Hagfeldt A and Grätzel M 2016 *Energy Environ. Sci.* **9** 1989

[20] Bu T L, Liu X P, Zhou Y, Yi J P, Huang X, Luo L, Xiao J Y, Ku Z L, Peng Y, Huang F Z, Cheng Y B and Zhong J 2017 *Energy Environ. Sci.* **10** 2509

[21] Bu T L, Li J, Zheng F, Chen W J, Wen X M, Ku Z L, Peng Y, Zhong J, Cheng Y B and Huang F Z 2018 *Nat. Commun.* **9** 4609

[22] Stone K H, Gold-Parker A, Pool V L, Unger E L, Bowring A R, McGehee M D, Toney M F and Tassone C J 2018 *Nat. Commun.* **9** 3458

[23] Kim M J, Kim G H, Lee T K, Choi I W, Choi H W, Jo Y, Yoon Y J, Kim J W, Lee J, Huh D, Lee H, Kwak S K, Kim J Y and Kim D S 2019 *Joule* **3** 2179

[24] Wu Y Z, Islam A, Yang X D, Qin C J, Liu J, Zhang K, Peng W Q and Han L Y 2014 *Energy Environ. Sci.* **7** 2934

[25] Wei D, Wang T Y, Ji J, Li M C, Cui P, Li Y Y, Li G Y, Mbengue J M and Song D D 2016 *J. Mater. Chem. A* **4** 1991

[26] Hu Y, Si S, Mei A Y, Rong Y G, Liu H W, Li X and Han H W 2017 *Sol. RRL* **1** 1600019

[27] Zhou Y Y, Yang M J, Kwun J, Game O S, Zhao Y X, Pang S P, Padture N P and Zhu K 2016 *Nanoscale* **8** 6265

[28] Yi C Y, Li X, Luo J S, Zakeeruddin S M and Grätzel M 2016 *Adv. Mater* **28** 2964

[29] Wang Y F, Li S B, Zhang P, Liu D T, Gu X L, Sarvari H, Ye Z B, Wu J, Wang Z M and Chen Z D 2016 *Nanoscale* **8** 19654

[30] Bi D Q, Yi C Y, Luo J S, Décoppet J D, Zhang F, Zakeeruddin S M, Li X, Hagfeldt A and Grätzel M 2016 *Nat. Energy* **1** 16142

[31] Li F C, Yuan J Y, Ling X F, Zhang Y N, Yang Y G, Cheung S H, Ho C H Y, Gao X Y and Ma W L 2018 *Adv. Funct. Mater* **28** 1706377

[32] Liu C, Tu J, Hu X T, Huang Z Q, Meng X C, Yang J, Duan X P, Tan L C, Li Z and Chen Y W 2019 *Adv. Funct. Mater* **29** 1808059

[33] Bai Y, Lin Y, Ren L, Shi X L, Strounina E, Deng Y H, Wang Q, Fang Y J, Zheng X P, Lin Y Z, Chen Z G, Du Y, L, Wang L Z and Huang J S 2019 *ACS Energy. Lett.* **4** 1231

[34] Wang D, Zhang L, Deng K M, Zhang W N, Song J, Wu J H and Lan Z 2018 *Energy Technol.* **6** 2380

[35] Zhang X Z, Zhang W N, Wu T Y, Wu J H and Lan Z 2019 *Sol. Energy* **181** 293

[36] Yu Z H, Chen B L, Liu P, Wang C H, Bu C H, Cheng N, Bai S H, Yan Y F and Zhao X Z 2016 *Adv. Funct. Mater* **26** 4866

[37] Chen H, Li K M, Liu H, Gao Y L, Yuan Y B, Yang B C and Zhou C H 2018 *Org Electron.* **61** 119